Robust Fat Suppression at 3T in High-Resolution Diffusion-Weighted Single-Shot Echo-Planar Imaging of Human Brain

Joelle E. Sarlls,[1,2]* Carlo Pierpaoli,[3] S. Lalith Talagala,[2] and Wen-Ming Luh[4]

Single-shot echo-planar imaging is the most common acquisition technique for whole-brain diffusion tensor imaging (DTI) studies in vivo. Higher field MRI systems are readily available and advantageous for acquiring DTI due to increased signal. One of the practical issues for DTI with single-shot echo-planar imaging at high-field is incomplete fat suppression resulting in a chemically shifted fat artifact within the brain image. Unsuppressed fat is especially detrimental in DTI because the diffusion coefficient of fat is two orders of magnitude lower than that of parenchyma, producing brighter appearing fat artifacts with greater diffusion weighting. In this work, several fat suppression techniques were tested alone and in combination with the goal of finding a method that provides robust fat suppression and can be used in high-resolution single-shot echo-planar imaging DTI studies. Combination of chemical shift saturation with slice-select gradient reversal within a dual-spin-echo diffusion preparation period was found to provide robust fat suppression at 3 T. Magn Reson Med 66:1658–1665, 2011. © 2011 Wiley Periodicals, Inc.

Key words: mri; diffusion; fat suppression; brain; artifact

As technical advances allow clinical application in MRI to move toward higher field strengths, the increased signal-to-noise ratio can be exploited to improve the resolution of in vivo imaging. This is especially attractive for diffusion-weighted and diffusion tensor imaging (DTI), as higher-resolution provides a finer sampling of tissue from which to extract diffusion properties. Typically, DTI data are acquired with a diffusion-weighted single-shot echo-planar imaging sequence (SSEPI) due to its time efficiency and insensitivity to motion induced phase errors. Good quality SSEPI images of human brain can readily be acquired at 2×2 mm^2 in-plane resolution or higher by using parallel imaging techniques, such as Sensitivity Encoding (SENSE) and Generalized Autocalibrating Partially Parallel Acquisition (GRAPPA).

In SSEPI used for DTI analysis, it is advisable to aim at isotropic voxels rather than increasing disproportionately in-plane resolution to achieve higher resolution. The intravoxel orientational coherence of white matter fibers is an important determinant of measured anisotropy (1) and apparent fiber orientation, so acquiring images with isotropic voxel dimensions insures a balanced weighting of architectural features of white matter in all directions (2). Therefore, the minimum achievable slice thickness may constrain the isotropic voxel dimensions that can be achieved for high-resolution DTI. In addition, signal from fat must be fully suppressed in SSEPI DTI as it produces a chemically shifted image that overlaps the tissue of interest and the diffusion coefficient for fat is very low, i.e., approximately 1×10^{-5} mm^2/s (3), and therefore biasing the diffusion properties of the underlying tissue.

Several fat suppression methods have been used in SSEPI DTI. These methods include chemical shift selective pulse and saturation (CS) (4) and spectral inversion-recovery (5). These methods require a preparation period with a chemical shift selective radiofrequency (RF) pulse centered on the precessional frequency of fat with a narrow bandwidth (BW), leaving the water signal unaffected. CS and spectral inversion-recovery are sensitive to both amplitude of static (polarizing) field (B_0) and amplitude of (excitation) radiofrequency field (B_1) inhomogeneities (6). Effects of B_0 field inhomogeneity are more severe at higher field strengths, near air/tissue interfaces, and at the edge of the head where fat is located. Therefore, the frequency of fat can be shifted outside the effective BW of the RF pulse used to excite or invert the fat signal. In addition, it is known that B_1 is inhomogeneous at higher field strengths due to dielectric effects (7). Accordingly, in practice, fat suppression by these techniques is commonly incomplete.

Spatial-spectral excitation (SPSP) (8,9) has been used in SSEPI acquisitions (10) as a method to excite water within a slice without affecting fat. This method is more robust in suppressing fat at 3 T because the degree of suppression is not affected by B_1 inhomogeneities. However, SPSP is often limited in the minimum slice thickness that can be achieved due to gradient slew-rate and amplitude constraints. The minimum slice thickness achievable in the product diffusion sequence of clinical scanners that currently use SPSP is ~2.4 mm.

[1]Center for Neuroscience and Regenerative Medicine, Uniformed Services University of the Health Sciences, Bethesda, Maryland, USA.

[2]National Institute of Neurological Disorders and Stroke, NIH MRI Research Facility, National Institute of Neurological Disorders and Stroke, National Institutes of Health, Bethesda, Maryland, USA.

[3]Eunice Kennedy Shriver National Institute of Child Health and Human Development, Program on Pediatric Imaging and Tissue Sciences, Eunice Kennedy Shriver National Institute of Child Health and Human Development, National Institutes of Health, Bethesda, Maryland, USA.

[4]Functional MRI Facility, National Institute of Mental Health, National Institutes of Health, Bethesda, Maryland, USA.

Recently, techniques exploiting the difference in fat and water frequencies on slice selection have been proposed for fat suppression. Because of the difference in frequency, the fat slice is displaced from the water slice by

$$D = \frac{\delta B_0}{G} = \frac{\Delta\omega_{fat}}{\gamma G} \qquad [1]$$

where D is displacement in mm, δ is the relative chemical shift in ppm, B_0 is the main field strength in Tesla, G is the slice-select gradient amplitude in mT/m (11), and $\Delta\omega_{fat}$ is the shift in frequency of fat when compared with water. The ratio between fat displacement and slice thickness is given by

$$\frac{D}{\Delta S} = \frac{\Delta\omega_{fat}}{BW} \qquad [2]$$

where ΔS is slice thickness and BW is the RF pulse BW. In the case where two RF pulses are applied, a difference in BW results in different displacement for the affected fat slice. In addition, slice select gradients of opposite polarity will produce displacement of the fat slice in opposite directions (Eq. 1). To exploit these phenomena for fat suppression, the affected fat slices from different RF pulses should not overlap. Therefore, the general expression to be satisfied for fat suppression is given by

$$\frac{\Delta\omega_{fat}}{BW_1} + j\frac{\Delta\omega_{fat}}{BW_2} \geq 1 \qquad [3]$$

where BW_1 and BW_2 are the BWs of the first and second RF pulses, respectively, and $j = -1$ if corresponding slice select gradients are of the same polarity and $j = 1$ for opposite polarity.

The slice-selection gradient reversal (SSGR) method (11,12) uses opposite polarity slice select gradients with equal BWs. This method has been proposed as an alternative fat suppression technique in a dual-spin-echo diffusion preparation period (13). A more recently proposed fat suppression technique uses different RF pulse durations, and hence different BWs, for excitation and refocusing with same polarity slice select gradients (14). This technique is well suited for higher field strengths, e.g., 7 T, because the frequencies of fat and water are further separated and it is low in specific absorption rate. The strategy of different BWs alone is not ideal at 3 T as the pulse durations needed for complete fat suppression would require a substantial increase in echo time (TE).

Accordingly, in this work we have focused on SSGR. However, many commercial sequences use slightly different BWs for excitation and refocusing, by adding a small contribution to fat suppression. For SSGR with slightly different BW_{90} and BW_{180} investigated in this work, complete fat suppression is achieved when the ratio between displacement and slice thickness for the $180°$ RF pulses, derived from Eq. 3, is

$$\frac{\Delta\omega_{fat}}{BW_{180}} \geq \left(1 - \frac{\Delta\omega_{fat}}{BW_{90}}\right) \qquad [4]$$

It follows that if the precessional frequency of fat is shifted toward lower frequencies, due to field inhomoge-

neity, the SSGR method will be even more effective. Although SSGR is a promising method for fat suppression at high-field, in practice, imperfections in the slice profile can degrade its performance.

In this work, the effectiveness of multiple stand-alone fat suppression techniques (CS, SPSP, and SSGR) and SSGR combined with CS (SSGR-CS) was evaluated with phantom and human data. The goal of the investigation was to determine the most complete and robust method of fat suppression that would allow the acquisition of high-resolution SSEPI DTI data with minimum fat artifacts.

MATERIALS AND METHODS

Data Acquisition

All data were collected on a 3-T HDx MRI system (GE Healthcare, Milwaukee, WI) with gradients capable of 40 mT/m. An SSEPI DTI sequence with a dual-spin-echo diffusion preparation period was adapted for SSGR by implementing opposite polarity slice-select gradients for the two $180°$ RF pulses, i.e., {+ + −} polarity for the $90°$, $180°$, and $180°$ RF pulses. The crusher gradients surrounding each $180°$ RF pulse were bridged to the slice-select gradients with the same polarity. The frequency of the second $180°$ RF pulse was adjusted to correspond with the negative polarity slice-select gradient such that off-center slices would be properly refocused. Informed consent was obtained for all subjects with a research protocol approved by the Institutional Review Board.

Phantom data were acquired with CS, SPSP, SSGR, and SSGR-CS and without fat suppression of a 7-cm diameter sphere filled with 50% polyvinylpyrrolidone (PVP) (15) immersed in a container of vegetable oil, along side a 15-cm diameter sphere filled with distilled water, using an eight-channel phased array coil. The sphere filled with distilled water allowed for the center frequency of water to be readily determined and for the PVP sphere in oil to be positioned toward the edge of the coil, corresponding to the normal fat location for in vivo imaging. The diffusion datasets, consisting of three non-diffusion-weighted images (non-DWIs) and 17 diffusion directions with a b-value $= 1100$ s/mm^2 were acquired with the following scan parameters: TE/pulse repetition time $= 85$ ms/5.9 s, slice thickness $= 2.5$ mm, matrix $= 96 \times 96$, field of view $= 24$ cm, acceleration factor $= 2$, $BW_{90} = 708$ Hz, and $BW_{180} = 905$ Hz. Incorporating the default BW_{90}, the ratio that needs to be satisfied from Eq. 4 is $\frac{\Delta\omega_{fat}}{BW_{180}} \geq 0.3956$ for on-resonance fat with $\Delta\omega_{fat} = 427.9$ Hz. Using the default BW_{180}, the ratio of $\frac{\Delta\omega_{fat}}{BW_{180}} \geq 0.473$. SSGR data were also acquired with the following additional BW_{180}/TE combinations and resulting ratios: 724 Hz/86.4 ms, 579 Hz/88.5 ms, and 482 Hz/90.5 ms with ratio $\frac{\Delta\omega_{fat}}{BW_{180}} = 0.591, 0.739,$ and 0.888, respectively. Note that all BW_{180} satisfy the condition from Eq. 4.

Data were acquired on healthy subjects using a receive-only 16-channel phased array coil (NOVA Medical, Wakefield, MA). The same scan parameters were used as the phantom acquisition, except pulse repetition time $= 18.5$ s to accommodate 60 slices. For comparison with the phantom data, one subject underwent scanning

with all sequence variations. Additionally, data were acquired with CS and SSGR-CS on five healthy subjects. The data sets contained six non-DWIs and 54 diffusion directions with maximum b-value = 1100 s/mm^2. One of the five additional subjects had data acquired with phase encoding in right/left, to verify change in the chemically shifted image. BW$_{180}$ was automatically calculated by the scanner software based on patient weight to minimize power deposition. For the five additional subjects scanned, the BW$_{180}$ varied from 905 to 579 Hz, resulting in $\frac{\Delta\omega_{fat}}{BW_{180}} = 0.473$ to 0.739, all of which satisfy the condition from Eq. 4.

The SSGR-CS sequence was also used to acquire data of a healthy volunteer at 1.7 mm isotropic voxel size. The data set also contained six non-DWIs and 54 diffusion directions with maximum b-value = 1100 s/mm^2 with the following scan parameters: TE/pulse repetition time = 91 ms/21 s, slice = 1.7 mm, 128 × 128, field of view = 22 cm, acceleration factor = 2, and BW$_{180}$ = 872 Hz.

Diffusion Tensor Image Processing

The diffusion data was processed using the TORTOISE software package available to download at www.tortoisedti.org (16). For in vivo data, the preprocessing steps include (1) rigid body motion correction, (2) eddy-current distortion correction, (3) B_0 distortion correction, and (4) bicubic upsampling to 1.5 mm isotropic resolution. For all diffusion data sets, the diffusion tensor (17) was computed by nonlinear least squares fitting. The orientationally averaged mean diffusivity, <D> (17), which is equal to 1/3 of the Trace of the diffusion tensor, and the fractional anisotropy (FA) (18) were calculated on a voxel-by-voxel basis. Conventional directionally encoded color maps were also derived from the DTI data (19).

Quantitative Analysis

If residual fat is present in diffusion-weighted data, the <D> will be decreased proportionally. Accordingly, <D> was analyzed to determine the effectiveness of fat suppression. For phantom data, <D> was measured for each acquisition in a PVP region-of-interest (ROI-PVP) placed in the lower half of the ball, avoiding the fat artifact, and a ROI (ROI-fat) encompassing the well defined fat artifact in the "No Fat Sat" data (Fig. 1D). Similarly, for in vivo data acquired with all sequence variations, <D> was measured for each acquisition within a ROI-fat that was created from the data acquired without fat suppression. A diffusion-weighted volume, containing all slices, from the No Fat Sat data set was masked to remove nonbrain voxels with a threshold at 35% maximum signal intensity, and manually masked to remove spurious voxels outside of the fat artifact. The average <D> for the whole brain was also measured, excluding all cerebrospinal fluid contaminated voxels with <D> above 1000×10^{-12} m^2/s.

<D> was also measured for the in vivo data acquired on five subjects in both ROI-fat and the whole brain. In this case, ROI-fat was created by subtracting a diffusion-weighted SSGR-CS volume from the corresponding CS volume. The subtracted volume was masked to remove nonbrain voxels with a threshold at 35% of the maximum residual fat signal, and manually masked to remove spurious voxels outside the fat artifact. Normalized difference images were also calculated from the <D> maps as ((CS − SSGR-CS)/CS) to highlight the residual fat signal in CS.

RESULTS

Figure 1A shows DWIs and calculated <D> maps from the phantom data collected with various fat suppression methods. The effect of the fat signal can be clearly seen in the No Fat Sat data. In the calculated maps of this homogeneous phantom, the artifact due to unsuppressed fat signal generally manifests as decreased <D> within the PVP sample. The decrease in <D> is expected as fat has a lower <D> than the PVP sample. Using the CS fat suppression method, the effect of residual fat signal can be seen in the <D> map. In the images acquired with SSGR, the fat signal that was residual with the CS method has been significantly removed; however, a different region of residual fat is present. As the ratio $\frac{\Delta\omega_{fat}}{BW_{180}}$ increases, the amount of residual fat decreases. Using combined SSGR-CS most chemically shifted fat signals have been removed, similar to data acquired with the SPSP excitation pulse. Figure 1B shows a plot of measured values from the ROIs. The <D> measured from ROI-PVP is similar for all acquisitions. In the ROI-fat, there is a reduction in <D> for the acquisitions that contain residual fat. Both SSGR-CS and SPSP have <D> values in ROI-fat that are most similar to <D> in ROI-PVP, indicating good fat suppression.

Figure 2 shows the equivalent analysis for the in vivo data. In Fig. 2A, the residual fat can be seen as increased signal in the DWIs and a decrease in the <D> maps. From the ROI analysis of all slices, shown in Fig. 2B, it can be seen that CS and SSGR had the most residual fat, resulting in the greatest decrease in <D> when compared with brain tissue. In SSGR, as the ratio $\frac{\Delta\omega_{fat}}{BW_{180}}$ increases the fat suppression improves and seems to fully suppress fat at a ratio of 0.888. SSGR-CS and SPSP also have <D> values in ROI-fat that are similar to the average <D> of the brain tissue.

In Fig. 3, DWIs, <D> maps, and normalized difference images are shown for the five healthy volunteers acquired with both CS and SSGR-CS. With CS, unsuppressed fat can be clearly seen as a bright ring running through the frontal lobes in the first four subjects and through the left hemisphere in subject 5. In subject 5, the shift in the artifact was due to the change in phase encoding direction, consistent with the expected behavior of fat signal. The fat signal produces a decrease in <D> for the CS data. Although not always prominent in the <D> map, the normalized difference image between <D> of CS and SSGR-CS more clearly reveals the artifact. Table 1 summarizes the measured ROI-fat results. The average in <D> for ROI-fat of the CS data varies between subjects and is significantly reduced when compared with the average <D> for the brain ($P = 0.035$, paired t-test). In contrast, the average <D> in ROI-fat for the SSGR-CS data is similar to the average <D> for the
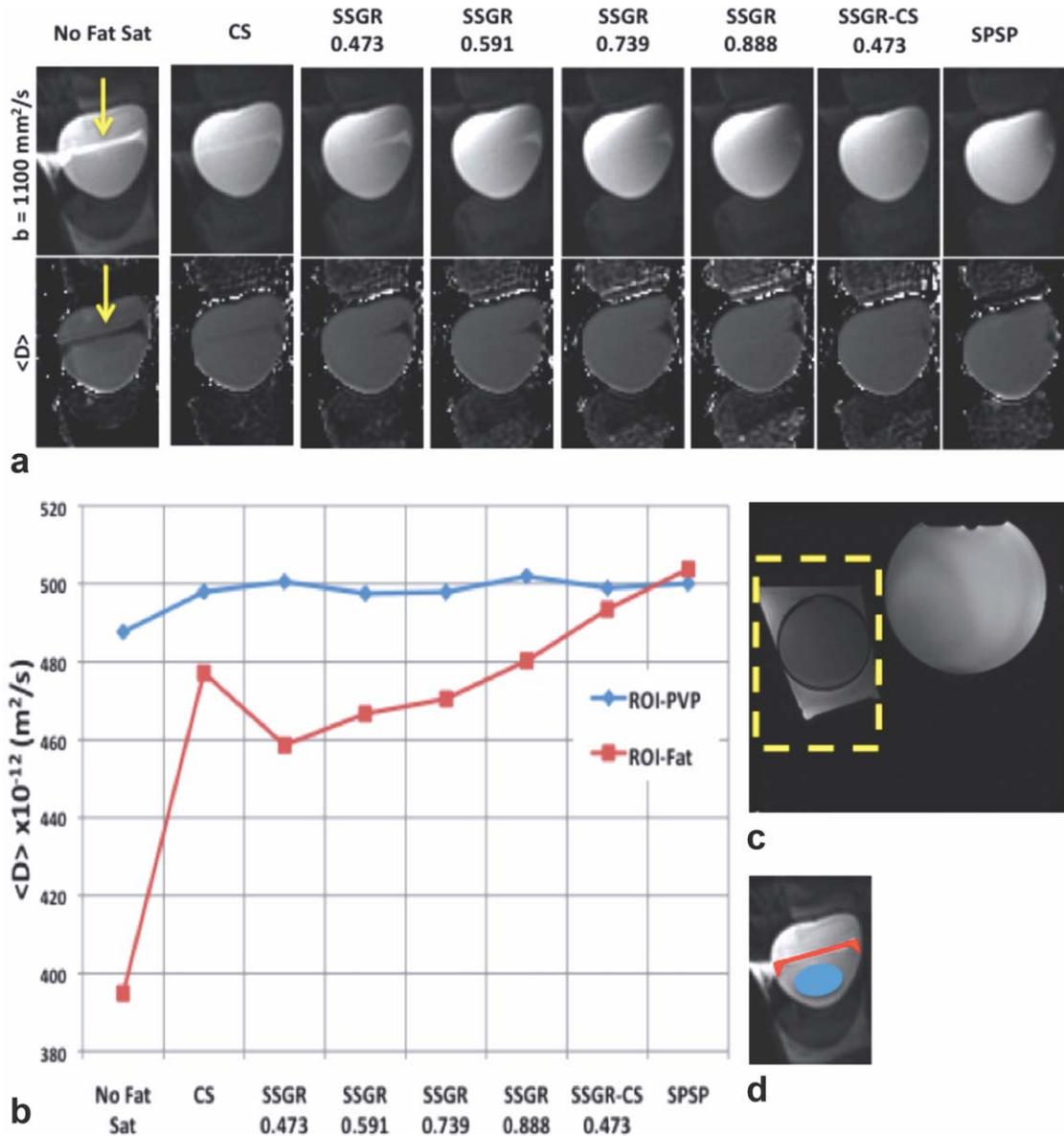
FIG. 1. **a**: Cropped region of representative images from *b*-value = 1100 (top row) and <D> maps (bottom row). The SSGR labels are the $\frac{\Delta\omega_{fat}}{BW_{180}}$ ratio values, whereas the yellow arrows indicate residual fat signal. **b**: Mean values from the ROI encompassing the fat (ROI-fat) and the ROI encompassing PVP (ROI-PVP). **c**: Reference image with an outline of the cropped region shown in (a). **d**: Illustration showing the placement of ROI-fat and ROI-PVP used to calculate the values graphed in (b).

brain in all subjects ($P = 0.89$, paired *t*-test). This shows that SSGR-CS provides superior fat suppression when compared with CS. Additionally, although weight varies between subjects, its value is not correlated to <D> in ROI-fat of the CS data ($r = 0.12$).

Figure 4 shows representative FA maps and normalized difference images of subject #1, 2, and 3, corresponding to data in Fig. 3, cropped to the region containing the fat artifact. The fat artifact can be seen in the CS FA maps. The fat artifact causes a substantial increase in FA, for those voxels with low FA. Conversely, in the areas of white matter with underlying high FA, the fat artifact causes a decrease in the calculated FA. A closer look at images from the individual diffusion directions reveals that the fat artifact is not homogeneous in intensity, and varies slightly in loca-tion along the phase-encoding direction depending on the applied diffusion direction. Both inhomogeneous artifact intensity and unstable location will vary the intensity in an affected voxel between diffusion directions, producing an overestimation of FA for voxels with underlying low FA. Two contributing factors may lead to an underestimation of FA for voxels with underlying high FA: (1) the signal from fat is isotropic and (2) the inconsistent intensity of the fat signal obscures the systematic change in signal intensity for highly anisotropic tissue with diffusion direction. This opposing effect is more clearly seen in the normalized difference images. The brightest voxels in the fat artifact of the third column are about a 60% overestimation, while the darkest voxels are about a 50% underestimation in FA.
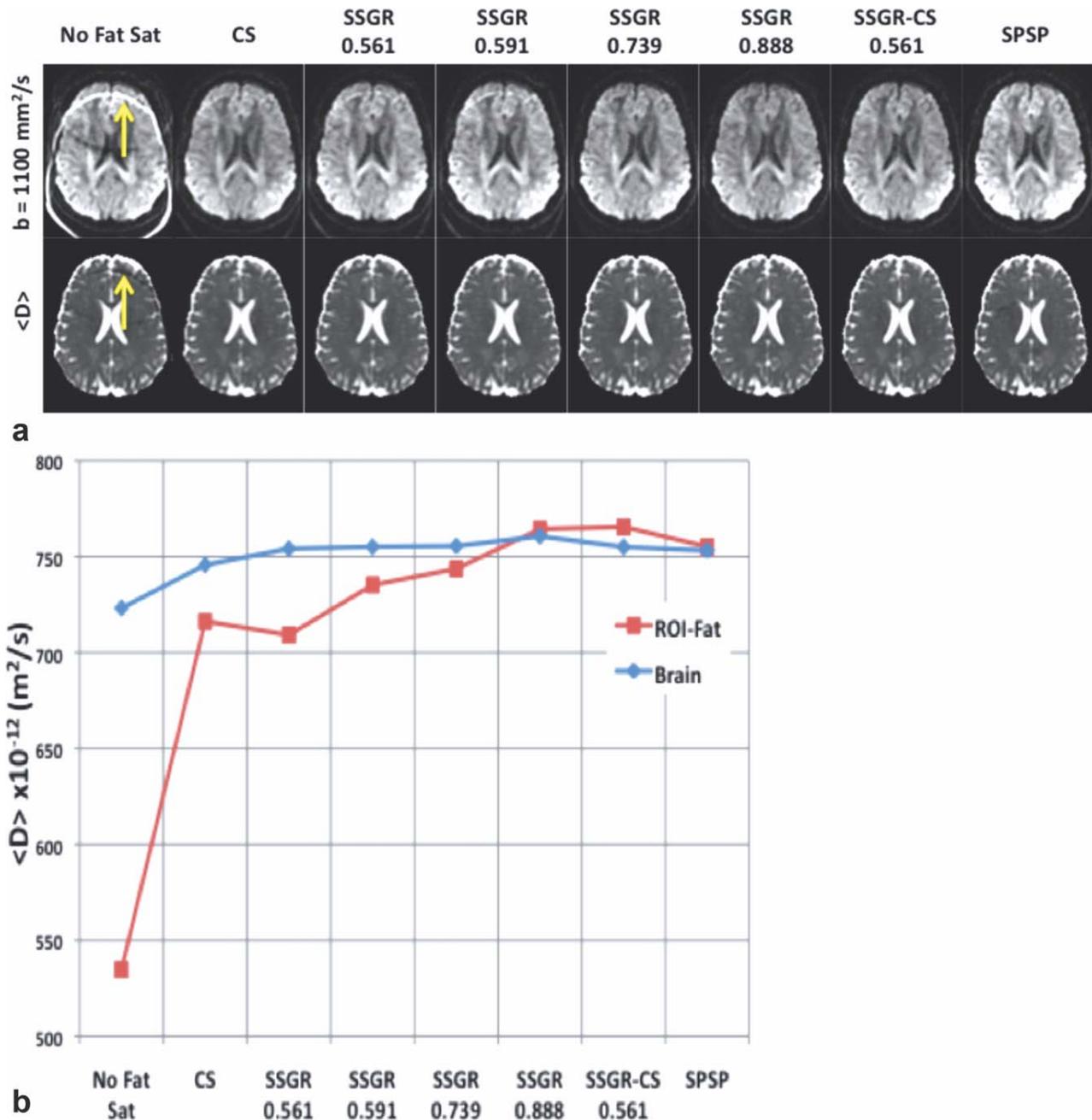
FIG. 2. **a**: Representative slice from the b-value $= 1100$ images (top row) and the $\langle D \rangle$ maps (bottom row). The SSGR labels are the $\frac{\Delta\omega_{fat}}{BW_{180}}$ ratio values, whereas the yellow arrows indicate residual fat signal. **b**: Plot of the mean values from the whole brain ROI-fat and the average over all brain tissue.

Figure 5 shows representative slices from all levels of the brain for data acquired with 1.7 mm isotropic resolution using the SSGR-CS method. These images demonstrate that high-resolution whole-brain DTI data can be acquired without fat artifacts using the SSGR-CS method. Because of the high resolution, several fine architectural features can be distinguished and have reduced partial volume effects when compared with typical 2.5 mm isotropic resolution images. For example, the optic tracts (white arrow) and additional subcortical white matter (yellow arrows) are discernable and have diffusion properties closer to that of uncontaminated white matter.

DISCUSSION

The combination of SSGR and traditional CS, SSGR-CS, is shown to be a robust method of fat suppression. Although additional time is required to accommodate the CS preparation period it does not increase the overall scan time for DTI acquisitions, as the main factor limiting scanning speed is the duty cycle of the gradients. In fact, overall scan time is slightly reduced using SSGR-CS when compared with SPSP, as SPSP excitation requires multiple high amplitude slice-select gradient pulses.

The SSGR method showed improved fat suppression, as the ratio was increased, resulting in complete
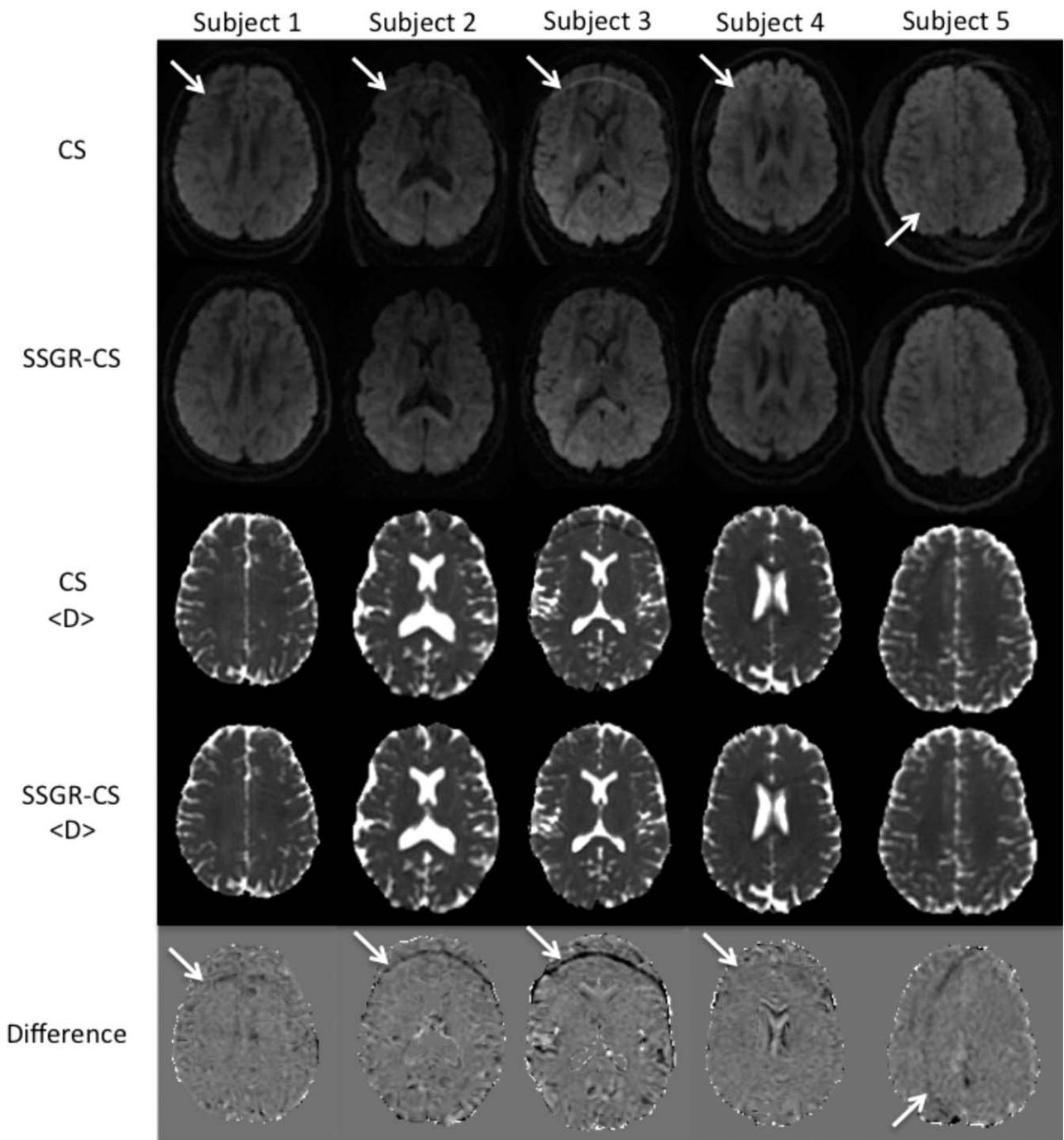
FIG. 3. DWIs with *b*-value = 1100 s/mm^2, <D> maps, and normalized difference images from five volunteers collected with CS and SSGR-CS. The data acquired on the fifth subject has phase encoding in R/L. White arrows indicate the residual fat artifact.

Table 1
Summary of the Whole Brain Analysis of the Five Subjects. All <D> × 10–12m^2/s

| Subject	Weight (kg)	$\frac{\Delta\omega_{fat}}{BW_{180}}$	Voxels in ROI	ROI-fat <D> CS	ROI-fat <D> SSGR-CS	Brain <D> CS	Brain <D> SSGR-CS	Normalized difference
1	114	0.738	1694	722.31	759.27	760.23	762.22	−6%
2	89	0.586	1707	615.81	725.953	741.62	748.85	−15%
3	92	0.594	3787	615.67	759.79	758.39	769.73	−25%
4	82	0.535	1042	697.63	740.4	717.21	720.61	−6%
5	68	0.473	651	695.46	767.59	752.57	756.78	−11%
Mean ± st.dev	88.9 ± 16.8	0.585 ± 0.098	1776 ± 1210	669.3 ± 50.1	750.6 ± 17.0	746.0 ± 17.6	751.6 ± 18.9	−12.6 ± 7.9
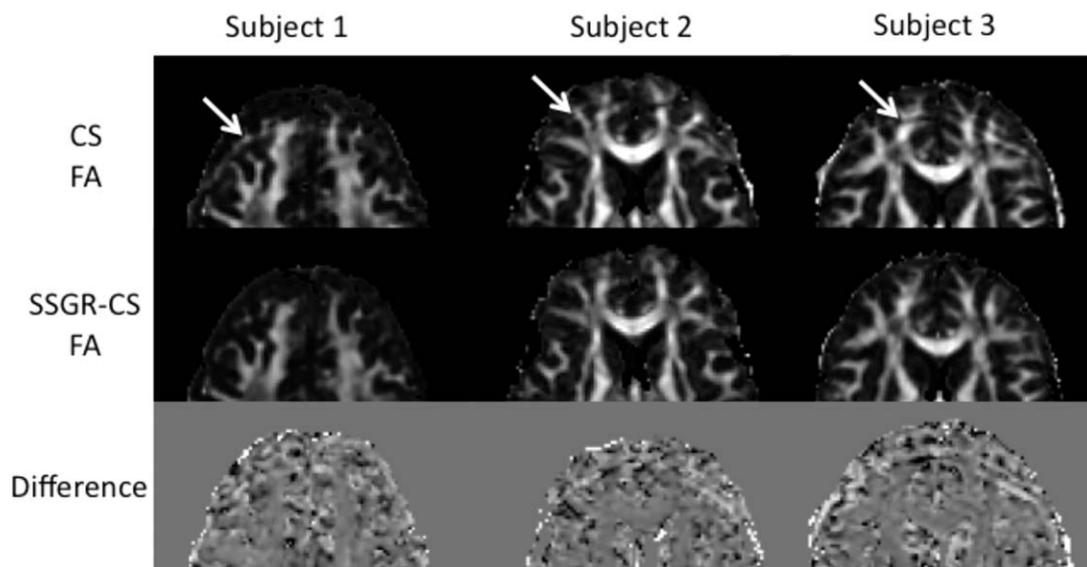
FIG. 4. FA maps and normalized difference images corresponding to the data shown in Fig. 3 for subject # 1, 2, and 3. Images have been cropped to the area containing the fat artifacts, indicated by white arrows.
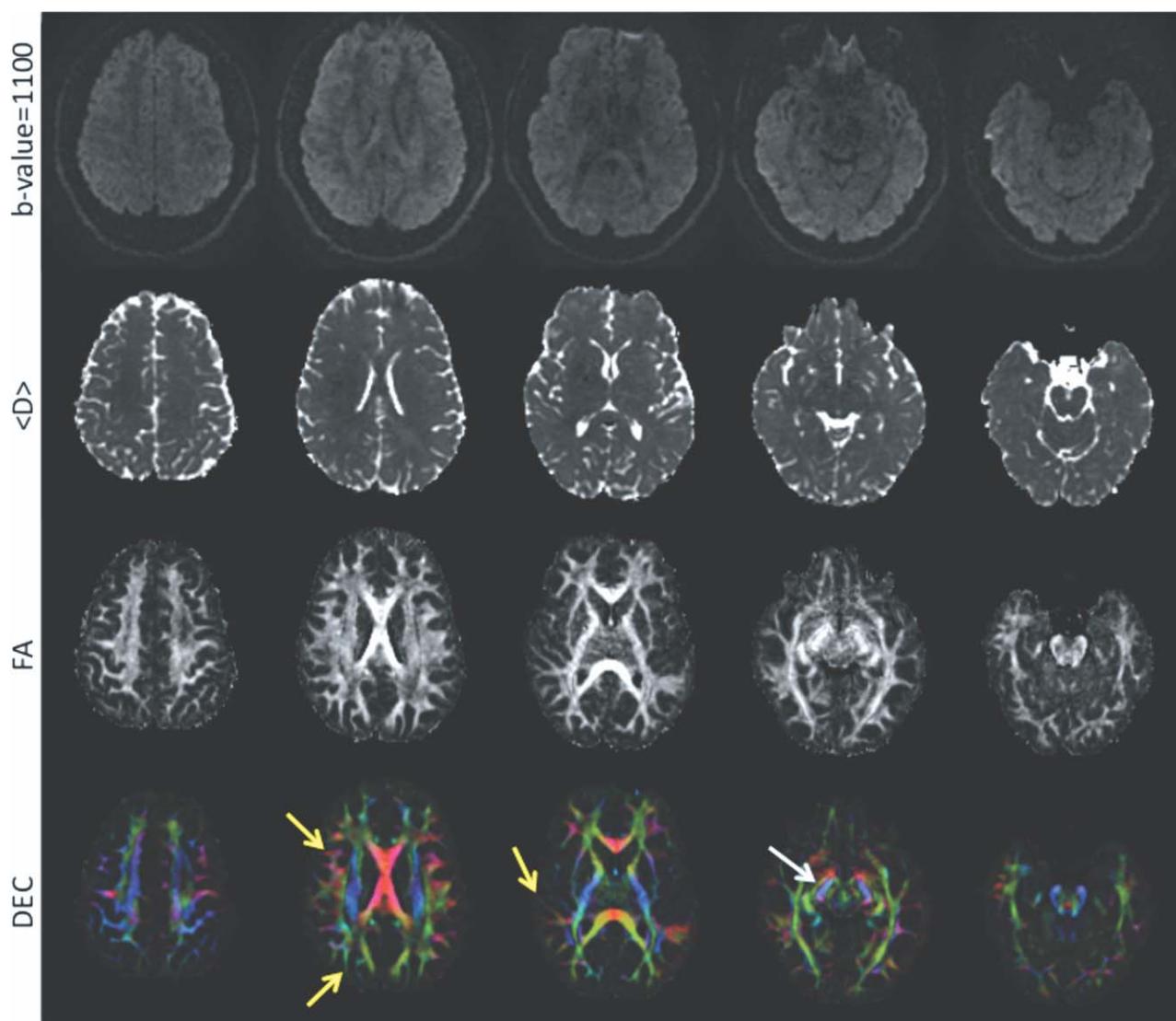

FIG. 5. Five slices from a whole brain SSEPI DTI acquisition at 1.7 mm isotropic voxel size. DWIs (top row), calculated <D> maps (second row), calculated FA (third row), and directionally encoded color maps (bottom row) are displayed. The yellow arrows point to subcortical white matter, whereas the white arrow points to the optic tract on the left side.

suppression at $\frac{\Delta\omega_{fat}}{BW_{180}} = 0.888$, with $BW_{180} = 482$ Hz, in the in vivo data. However, TE increases with the ratio, and BW_{180} decreases; a greater than 5 ms increase in TE for BW = 482 Hz as compared to the default 905 Hz for CS and SSGR-CS. In addition, an undesired effect of SSGR methods is the suppression of off-resonance water signal. Areas of greatest susceptibility, and thus off-resonance, are typically near air/tissue interfaces such as the paranasal sinuses and the mastoid air cells next to the inferior aspects of the frontal and temporal lobes, respectively. This undesirable effect is magnified as the BW_{180} decreases (Fig. 1A). For the BW_{180} used in SSGR-CS, the degree of off-resonance water signal suppression is similar to that of SPSP. Therefore, the SSGR-CS method is recommended due to its robust suppression of fat, minimum TE, and minimum suppression of off-resonance water.

Unsuppressed fat signal corrupts the diffusion properties of the underlying tissue of interest. The fat artifacts will typically result in an underestimation of <D> and in either an overestimation or an underestimation of FA, depending on the consistency of the artifact in different DWIs and the degree of anisotropy of the tissue. Both overestimating and underestimating FA are problematic for further data analysis and/or processing of the diffusion MRI data. This is especially true for fiber tracking: an underestimation of FA may result in premature termination of tracts, as low anisotropy is commonly used as a stopping criterion; whereas, an overestimation of FA may create spurious tracts that do not correspond to an anatomical structure. For <D>, it is important to note that the effect of the fat artifact, with a high signal intensity in DWIs and low <D>, is analogous to that of acute ischemia (20).

The dual-spin-echo preparation is most desirable to use for diffusion imaging, as it is known to reduce eddy-current effects (21). Accordingly, the SSGR method was used in a dual-spin-echo diffusion preparation. However, the SSGR method has been proposed in conjunction with a spin-echo type of diffusion preparation, where the polarity of the slice-select gradient for the 90° RF excitation pulse has opposite polarity as the slice-select gradient for the 180° RF refocusing pulse (12,22).

Although not presented in this work, it seems probable that the SSGR-CS method may also be effective in robustly suppressing fat in diffusion-weighted imaging in the body.

CONCLUSION

By combining the traditional CS fat suppression method with the SSGR fat suppression method during a dual-spin-echo diffusion preparation period, higher resolution SSEPI images with isotropic voxel dimensions can be acquired with minimum fat artifacts. By combining the two methods, both on and off-resonance fat signal is suppressed. Using such a sequence allows the greater signal available at higher fields to be exploited for increasing the resolution of SSEPI acquisitions.

REFERENCES

1. Pierpaoli C, Jezzard P, Basser PJ, Barnett A, Di Chiro G. Diffusion tensor MR imaging of the human brain. Radiology 1996;201:637–648.
2. Pierpaoli C. Artifacts in diffusion MRI. In: Jones DK editor. Diffusion MRI: theory, methods, and applications. New York: Oxford University Press; 2011.
3. Lehnert A, Machann J, Helms G, Claussen CD, Schick F. Diffusion characteristics of large molecules assessed by proton MRS on a whole-body MR system. Magn Reson Imaging 2004;22:39–46.
4. Haase A, Frahm J, Hanicke W, Matthaei D. ^{1}H NMR chemical shift selective (CHESS) imaging. Phys Med Biol 1985;30:341–344.
5. Kaldoudi E, Williams SCR, Barker GJ, Tofts PS. A chemical shift selective inversion recovery sequence for fat-suppressed MRI: theory and experimental validation. Magn Reson Imaging 1993;11:341–355.
6. Bley TA, Wieben O, François CJ, Brittain JH, Reeder SB. Fat and water magnetic resonance imaging. J Magn Reson Imaging 2010;31:4–18.
7. Yang QX, Wang J, Zhang X, Collins CM, Smith MB, Liu H, Zhu XH, Vaughan JT, Ugurbil K, Chen W. Analysis of wave behavior in lossy dielectric samples at high field. Magn Reson Med 2002; 47:982–989.
8. Meyer CH, Pauly JM, Macovski A, Nishimura DG. Simultaneous spatial and spectral selective excitation. Magn Reson Med 1990;15: 287–304.
9. Zur Y. Design of improved spectral-spatial pulses for routine clinical use. Mag Reson Med 2000;43:410–420.
10. Schick F, Forster J, Machann J, Kuntz R, Claussen CD. Improved clinical echo-planar MRI using spatial-spectral excitation. J Magn Reson Imag 1998;8:960–967.
11. Gomori JM, Holland GA, Grossman RI, Gefter WB, Lenkinski RE. Fat suppression by section-select gradient reversal on spin-echo MR imaging. Work in progress. Radiology 1988;168:493–495.
12. Volk A, Tiffon B, Mispelter J, Lhoste JM. Chemical shift-specific slice selection. A new method for chemical shift imaging at high magnetic field. J Magn Reson 1987;71:168–174.
13. Nagy Z, Weiskopf N. Efficient fat suppression by slice-selection gradient reversal in twice-refocused diffusion encoding. Magn Reson Med 2008;60:1256–1260.
14. Ivanov D, Schafer A, Streicher MN, Heidemann RM, Trampel R, Turner R. A simple low-SAR technique for chemical-shift selection with high-field spin-echo imaging. Magn Reson Med 2010;64: 319–326.
15. Pierpaoli C, Sarlls JE, Nevo U, Basser PJ, Horkay F. Polyvinylpyrrolidone (PVP) water solutions as isotropic phantoms for diffusion MRI studies. In: 17th Annual Proceedings of ISMRM, Honolulu; 2009. p 1414.
16. Pierpaoli C, Walker L, Irfanoglu MO, Barnett A, Basser P, Chang LC, Koay CG, Pajevic S, Rohde G, Sarlls J, Wu M. TORTOISE: an integrated software package for processing of diffusion MRI data. In: 18th Annual Proceedings of ISMRM, Stockholm; 2010. p 1597.
17. Basser PJ, Mattiello J, LeBihan D. Estimation of the effective self-diffusion tensor from the NMR spin-echo. J Magn Reson Ser B 1994; 103:247–254.
18. Basser PJ, Pierpaoli C. Microstructural and physiological features of tissues elucidated by quantitative-diffusion-tensor MRI. J Magn Reson Ser B 1996;111:209–219.
19. Pajevic S, Pierpaoli C. Color schemes to represent the orientation of anisotropic tissues from diffusion tensor data: application to white matter fiber tract mapping in the human brain. Magn Reson Med 1999;42:526–540.
20. Warach S, Gaa J, Siewert B, Wielopolski P, Edelman RR. Acute human stroke studied by whole brain echo planar diffusion-weighted magnetic resonance imaging. Ann Neurol 1995;37:231–241.
21. Reese TG, Heid O, Weisskoff RM, Wedeen VJ. Reduction of eddy-current-induced distortion in diffusion MRI using a twice-refocused spin echo. Magn Reson Med 2003;49:177–182.
22. Butts K, de Crespigny A, Pauly JM, Moseley M. Diffusion-weighted interleaved echo-planar imaging with a pair of orthogonal navigator echoes. Magn Reson Med 1996;35:763–770.